Drug Delivery

International Edition: DOI: 10.1002/anie.201909870
German Edition: DOI: 10.1002/ange.201909870

A DNA–Azobenzene Nanopump Fueled by Upconversion Luminescence for Controllable Intracellular Drug Release

Yue Zhang, Yue Zhang, Guobin Song, Yuling He, Xiaobo Zhang, Ying Liu, and Huangxian Ju**

Dedicated to the 100th anniversary of the School of Chemistry and Chemical Engineering, Nanjing University

Abstract: *Stimulus-responsive drug release possesses considerable significance in cancer therapy. This work reports an upconversion-luminescence-fueled DNA–azobenzene nanopump for rapid and efficient drug release. The nanopump is constructed by assembling the azobenzene-functionalized DNA strands on upconversion nanoparticles (UCNPs). Doxorubicin (DOX) is loaded in the nanopump by intercalation in the DNA helix. Under NIR light, the UCNPs emit both UV and visible photons to fuel the continuous photoisomerization of azo, which acts as an impeller pump to trigger cyclic DNA hybridization and dehybridization for controllable DOX release. In a relatively short period, this system demonstrates 86.7% DOX release. By assembling HIV-1 TAT peptide and hyaluronic acid on the system, targeting of the cancer-cell nucleus is achieved for perinuclear aggregation of DOX and enhanced anticancer therapy. This highly effective drug delivery nanopump could contribute to chemotherapy development.*

Chemotherapy remains the principal clinical antitumor strategy.[1] However, it often results in grievous toxic side effects due to the uncontrollable dose.[2] Stimulus-responsive drug-release systems can enhance drug accumulation in tumor tissues and eliminate off-target toxicity.[2b,3] Azobenzene (azo), which can reversibly isomerizes between *cis* and *trans* form under visible (Vis) and UV irradiation,[4] has been assembled on the surface of mesoporous nanoparticles[5] and microporous multilayer films[6] to act as a photoresponsive trigger for controlled drug release.

To improve release efficiency, some pump-type switchers[7,8] have been designed to accelerate the drug-release process. With the capability of simultaneously emitting photons in both UV and Vis regions upon near-infrared (NIR) irradiation,[9] upconversion nanoparticles (UCNPs) have been modified with azo[10] to continuously transform azo back and forth to propel drug release.[10a] In these UCNPs-azo nanodevices,[4a,10] azo is usually isolated from UCNPs, which weakens the luminescence-fueled efficiency. Therefore, these strategies need a long exposure time to release a drug in a satisfactory amount, which results in a thermal injury from continuous point-fixed irradiation.

To overcome this drawback, this work used azo-functionalized DNA strands to design a nanopump for efficient and controllable drug release. Flexible DNA chains could be compactly assembled on UCNPs[11] to act as the pump-type switcher triggered by the reversible conformational change of azo, which is conveniently fueled by Vis and UV irradiation emitted from the UCNPs. Moreover, the anticancer drug doxorubicin (DOX) could be selectively intercalated in a specific DNA helix[12] for highly efficient loading (Scheme 1 a). The continuous rotation-inversion movement of the phenyl moiety of azo in the hybridization zone of DNA backbones (DNA strands LA_{Azo}, LC_{Azo} with 3 azo moieties per DNA strand) determined the feasibility of the molecular impeller pump via DNA hybridization[13] and dehybridization to controllably release DOX upon NIR irradiation.

To diminish the active efflux of a drug by transporters like P-glycoprotein (P-gp) on cell membrane,[14] HIV-1 TAT, a nuclear localization peptide,[15] was conjugated to the DNA–azo nanopump for nuclear targeting (Scheme 1 b), which greatly enhanced the concentration of DOX in nuclear area, and thus improved therapeutic efficacy. Considering the need for cancer-cell targeting, anionic hyaluronic acid (HA) was also coated on the nanopump via electrostatic adsorption to specifically recognize CD44-overexpressing tumor cells to trigger HA-mediated endocytosis,[17] while hyaluronidase (HAase) in the tumor microenvironment[16] hydrolyzes HA to expose TAT for nuclear targeting (Scheme 1 c). The presence of HA coating prevented nonspecific interaction with serum components during delivery process,[18] and prevented the off-target effect. This work provides an ideal format for controllable drug release with high efficiency in cancer therapy.

$NaYF_4$:Tm,Yb core UCNPs containing 30% Yb^{3+} and 0.5% Tm^{3+} were synthesized using a reported procedure.[19] The $NaYF_4$ shell was deposited on the core to obtain core/shell-UCNPs, which compensated for surface defects and improved the optical properties of the UCNPs.[20] The core and core/shell-UCNPs showed monodispersed particle sizes of approximately 34 and approximately 41 nm, respectively (Figure 1 a,b). Their hexagonal crystal structures were confirmed by their powder X-ray diffraction patterns (Supporting Information, Figure S1). Under 980 nm laser irradiation, the

[*] Y. Zhang,[++] Y. Zhang,[+++] G. Song, Y. He, X. Zhang, Prof. Y. Liu, Prof. H. Ju
State Key Laboratory of Analytical Chemistry for Life Science, School of Chemistry and Chemical Engineering, Nanjing University
Nanjing 210023 (China)
E-mail: yingliu@nju.edu.cn
hxju@nju.edu.cn

[++] PhD candidate

[+++] MS candidate

Supporting information and the ORCID identification number(s) for the author(s) of this article can be found under: https://doi.org/10.1002/anie.201909870.

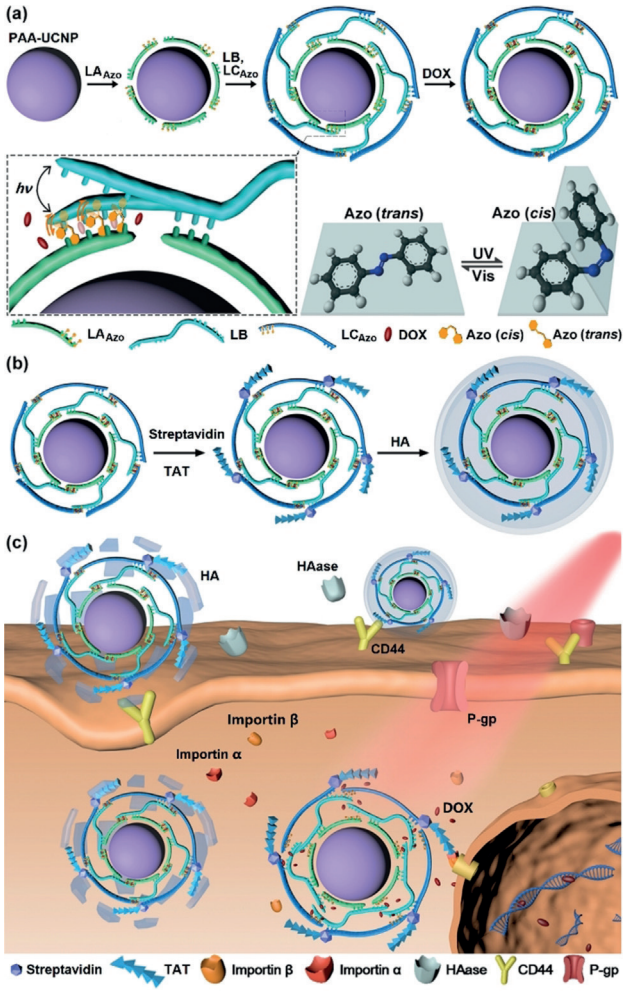

Scheme 1. Schematic illustration of a) UCNPs-LA$_{Azo}$BC$_{Azo}$/DOX assembly, b) UCNPs-LA$_{Azo}$BC$_{Azo}$/DOX-TAT-HA synthesis, and c) HA-mediated endocytosis, TAT-mediated nuclear targeting and NIR-triggered drug release in living cells. The enlarged section in (a) delineates the continuous photoisomerization of azo and cyclic hybridization and dehybridization of LA$_{Azo}$ and LB.

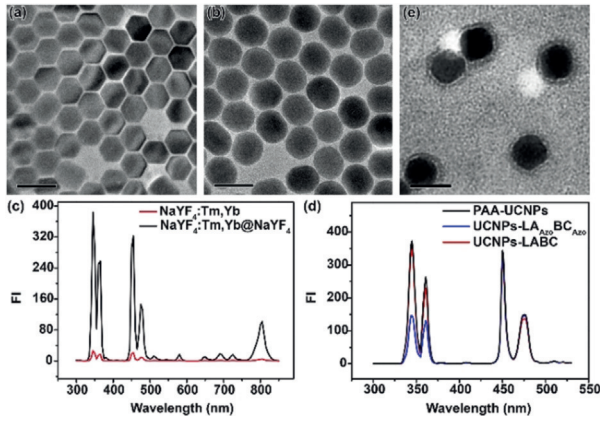

Figure 1. TEM images of a) NaYF$_4$:Tm,Yb and b) NaYF$_4$:Tm,Yb@NaYF$_4$. Upconversion luminescence spectra of c) NaYF$_4$:Tm,Yb and NaYF$_4$:Tm,Yb@NaYF$_4$ and d) PAA-UCNPs, UCNPs-LABC, and UCNPs-LA$_{Azo}$BC$_{Azo}$. e) TEM image of UCNPs-LABC stained with phosphotungstic acid (2 wt%, pH 6.5). The scale bar is 50 nm.

core/shell-UCNPs showed both UV (345 nm and 355 nm) and blue (455 nm and 475 nm) emissions with intensities about 15 times stronger than core UCNPs (Figure 1c).

After core/shell-UCNPs were modified with poly(acrylic acid) to form PAA-UCNPs via ligand exchange,[21] LA$_{Azo}$ was linked to PAA-UCNPs via amide bonding, and DNA strands LB and LC$_{Azo}$ were then assembled simultaneously through hybridization of LA$_{Azo}$ and LC$_{Azo}$ with each terminal of LB to form the DNA–azo nanopump (UCNPs-LA$_{Azo}$BC$_{Azo}$) (Supporting Information, Scheme S1),[22] which had a strong characteristic absorption of DNA at 260 nm and azo at 334 nm (Supporting Information, Figure S2). UCNPs-LA$_{Azo}$BC$_{Azo}$ showed decreased luminescence at 345 nm and 355 nm (Figure 1d). The assembly of three kinds of DNA strands showed gradually increased particle size (Supporting Information, Figure S3) and negative charge (Supporting Information, Figure S4), and produced a DNA layer with a thickness of about 9.5 nm (Figure 1e). To verify the assembly, DNA strands LA, LB, and LC were labeled with FAM, Cy3, and Cy5, respectively, to synthesize tricolor UCNPs-LA$_{FAM}$B$_{Cy3}$C$_{Cy5}$. From the fluorescence intensities and calibration curves, the ratio of assembled LA, LB, and LC was calculated to be 1.3:1:1, indicating sufficient hybridization of DNA strands on UCNPs (Supporting Information, Figure S5). The DNA dehybridization was confirmed through atomic force microscopic and circular dichroism measurements. Under visible-light exposure, the *trans* conformation of azo led to a 2.3 nm height of the DNA duplex strands (Supporting Information, Figure S6a) with a clear positive/negative Cotton effect at 272 nm (Supporting Information, Figure S6b), while the dehybridization upon *cis* isomerization of azo under UV light exposure led to a height of 0.5 nm and the disappearance of characteristic CD peak.

After DOX was loaded on UCNPs-LA$_{Azo}$BC$_{Azo}$ through its intercalation with DNA helix,[12,23] UCNPs-LA$_{Azo}$BC$_{Azo}$/DOX showed a characteristic absorption peak of DOX at 490 nm, while incubating DOX with LA$_{Azo}$ modified UCNPs (UCNPs-LA$_{Azo}$) did not produce obvious absorption (Supporting Information, Figure S7a), indicating little nonspecific adsorption in the absence of DNA duplex structure. The loading capacity was 14.6 μg DOX for 1 mg UCNPs-LA$_{Azo}$BC$_{Azo}$ with a loading efficiency of 58.4%, which were obtained from the fluorescence of DOX in supernatants before and after loading and the calibration curve of DOX (Supporting Information, Figure S7b,c). The capacity was comparable to previous reports.[24]

When UCNPs-LA$_{Azo}$BC$_{Azo}$/DOX were exposed to only UV light, the absorption peak of azo at 334 nm corresponding to the p–p* transition of the *trans* isomer[25] obviously decreased, and the absorption peak at 435 nm corresponding to the n–p* transition of the *cis* isomer[25] increased, while visible-light irradiation reversed the *cis* isomer into the *trans* isomer (Figure 2a). The continuous rotation-inversion movement of azo showed a dynamical balance under simultaneous UV/Vis irradiation, which produced a moderate absorption intensity. From the fluorescence intensities of DOX in supernatants and the calibration curve, the amounts of released DOX at different irradiation times could be obtained for evaluating the release efficiency of loaded DOX. Simul-

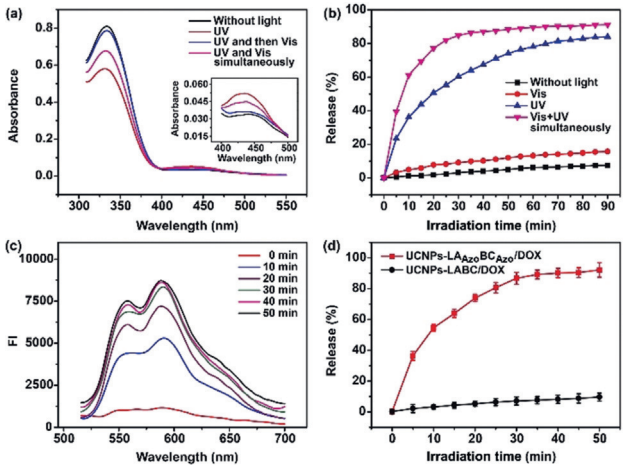

Figure 2. a) UV/Vis absorption spectra of UCNPs-LA$_{Azo}$BC$_{Azo}$ after exposed to UV, Vis, and UV/Vis light. Inset in (a): absorbance between 400 and 500 nm. b) Release percentages of DOX from UCNPs-LA$_{Azo}$BC$_{Azo}$/DOX after exposed to UV, Vis, and UV/Vis light. c) Fluorescence spectra for supernatants of UCNPs-LA$_{Azo}$BC$_{Azo}$/DOX for 0 to 50 min NIR irradiation. d) Release percentages of DOX from UCNPs-LA$_{Azo}$BC$_{Azo}$/DOX and UCNPs-LABC/DOX after 0 to 50 min NIR irradiation.

taneous UV/Vis irradiation showed much faster DOX release, and the release efficiency reached 84.9% within 30 minutes, at which UV or visible-light irradiation merely induced the release of 60.4% and 9.2% of DOX, respectively (Figure 2b). These results proved that the continuous conformational inversion of azo could effectively pump DOX out of the DNA nanodevice.

The upconversion-luminescence-fueled DOX release was examined with NIR exposure. With the increasing exposure time of UCNPs-LA$_{Azo}$BC$_{Azo}$/DOX, the fluorescence intensity of DOX in the supernatant increased, and reached the maximum value at 30 min (Figure 2c). The maximum release percentage was 86.7% (Figure 2d). The impressive release efficiency resulted from the continuous structural change of azo and the efficient azo–nanocarrier interaction.[26] Interestingly, the release efficiency of DOX was linearly related with the logarithm of NIR-irradiation time (Supporting Information, Figure S7d,e). The half time for DOX release was calculated as 8.45 min. As a control, the irradiation of UCNPs-LABC/DOX, assembled by hybridizing DNA strands LA, LB and LC around UCNPs with DOX loading, showed little fluorescence increase of DOX in the supernatant due to the absence of azo (Figure 2d and Supporting Information, Figure S8). These results indicate that the designed DNA–azo nanopump could efficiently control the release of DOX.

The stability of UCNPs-LA$_{Azo}$BC$_{Azo}$/DOX was investigated by examining DOX leakage upon incubation in 10% fetal bovine serum buffer, which was measured from the fluorescence intensity of DOX in the supernatant. During the incubation, the leakage percentage was less than 10% (Supporting Information, Figure S9), indicating the satisfactory stability of the DNA nanopump.

The therapeutic effect of drug released in the cytoplasm is generally decreased due to export of the drug by transporters in the cell membrane.[14,27] Endowing the DNA–azo nanopump with nuclear-targeting capacity can avoid the impairment and suppress multidrug resistance.[28] Thus, HIV-1 TAT was assembled on the nanopump,[29] which increased the hydrodynamic diameter (Supporting Information, Figures S3d and S10a) and Zeta potential (Supporting Information, Figure S10c). After anionic HA was introduced through electrostatic adsorption for specifically targeting cancer cells, the resulting nanopump had a hydrodynamic diameter of 118.8 nm (Supporting Information, Figure S10b) and a negative Zeta potential. The HA degradation upon incubation with HAase was demonstrated by the positive variation of Zeta potential (Supporting Information, Figure S10d). The HA-mediated endocytosis through the recognition of HA by CD44 was also validated from the confocal images. After incubation with FAM-labeled DNA nanopump, HepG2 cells showed strong fluorescence, while little fluorescence signal was observed when excessive HA coexisted in the culture medium (Supporting Information, Figure S11).

To demonstrate the TAT mediated nuclear-targeted transport, HepG2 cells were incubated with FAM-labeled UCNPs-LA$_{Azo}$BC$_{Azo}$-TAT-HA or UCNPs-LA$_{Azo}$BC$_{Azo}$-HA, and then stained with DAPI for nuclear identification. The former exhibited the fluorescence of FAM mainly in perinuclear region, while the fluorescence of the latter located in cytoplasm (Figure 3 and Supporting Information, Figure S12), indicating the important role of TAT in nuclear-targeted delivery.

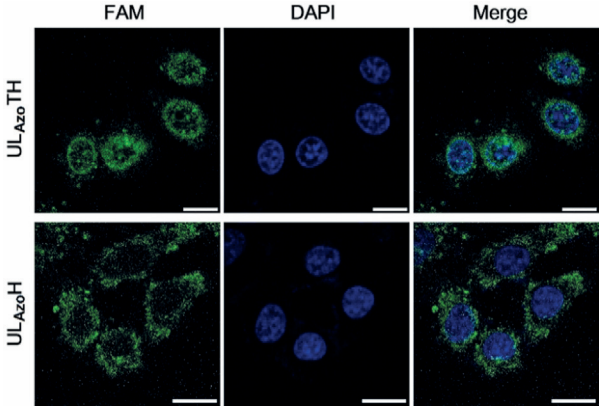

Figure 3. Confocal laser scanning microscopy (CLSM) images of HepG2 cells treated with FAM-labeled UCNPs-LA$_{Azo}$BC$_{Azo}$-TAT-HA (UL$_{Azo}$TH) and UCNPs-LA$_{Azo}$BC$_{Azo}$-HA (UL$_{Azo}$H). The scale bar is 25 μm.

The cellular therapeutic efficiency was firstly evaluated with a standard MTT assay. After 10 min NIR irradiation, the cells treated with UCNPs-LA$_{Azo}$BC$_{Azo}$/DOX-TAT-HA showed 43.5% suppression of cell proliferation, which reached 72.8% after 30 min NIR irradiation (Figure 4a), which were much stronger than those of 20% by azo-modified mesoporous silica[10a] and 60% by decomposable nanocapsules[4a] after 10 and 30 min NIR irradiation, respectively. In the

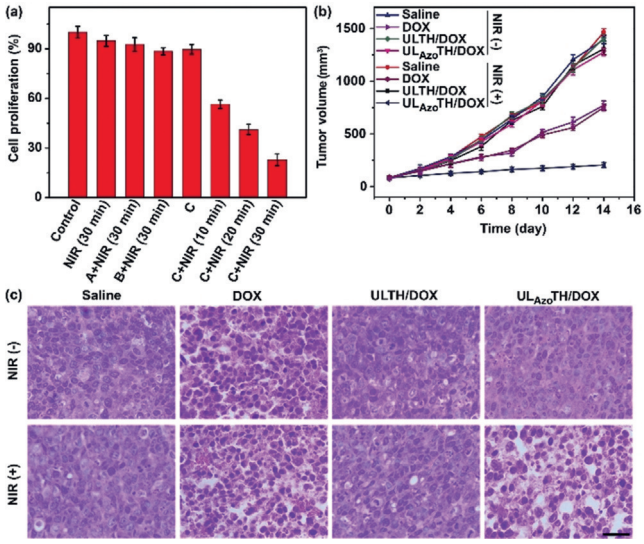

Figure 4. a) Relative cell proliferation percentages for HepG2 cells treated with UCNPs-LA$_{Azo}$BC$_{Azo}$-TAT-HA (A), UCNPs-LABC/DOX-TAT-HA (B), and UCNPs-LA$_{Azo}$BC$_{Azo}$/DOX-TAT-HA (C) and then NIR exposure. Error bars indicate mean ± SD (n = 3). b) Relative tumor volumes at different days after treatments. c) Histological observations of tumor tissues after treatment with saline, DOX, UCNPs-LABC/DOX-TAT-HA (ULTH/DOX), and UCNPs-LA$_{Azo}$BC$_{Azo}$/DOX-TAT-HA (UL$_{Azo}$TH/DOX), and then NIR irradiation. Error bars indicate mean ± SD (n = 5). The scale bar is 50 μm.

absence of either azo or NIR irradiation, the suppression was negligible. Furthermore, the treatment with UCNPs-LA$_{Azo}$BC$_{Azo}$-TAT-HA and then NIR irradiation showed little effect on both cell viability (Supporting Information, Figure S13) and morphology (Supporting Information, Figure S14), indicating negligible toxicity of both UCNPs-LA$_{Azo}$BC$_{Azo}$-TAT-HA and NIR irradiation to cells, as observed in previous work.[26b] Furthermore, the DNA–azo nanopump showed negligible influence on cell proliferation in the absence of NIR irradiation (Supporting Information, Figure S15), further confirming the stability of the nanopump. Similarly, the flow cytometric assay demonstrated cell apoptosis rates of 39.9%, 53.5%, and 71.1% upon the treatment with the proposed nanopump and NIR irradiation for 10, 20, and 30 min, respectively (Supporting Information, Figure S16). Therefore, the boosting effect of the DNA nanopump in accelerating the drug release greatly improved the anticancer therapeutics.

To demonstrate the advantage of nuclear targeting, HepG2 cells were incubated with DOX, UCNPs-LA$_{Azo}$BC$_{Azo}$/DOX-HA, and UCNPs-LA$_{Azo}$BC$_{Azo}$/DOX-TAT-HA at the same amount of DOX and irradiated with 980 nm laser (2 W cm^{-2}). UCNPs-LA$_{Azo}$BC$_{Azo}$/DOX-TAT-HA treated cells always showed the lowest cell proliferation at different DOX concentrations (Supporting Information, Figure S17), indicating the enhanced therapeutic efficacy of the nuclear-targeted drug delivery.

The performance of in vivo anticancer therapy was verified using mice bearing HepG2 xenograft tumors. The mice intratumorally injected with 150 μL DNA–azo nanopump and then irradiated with NIR for 30 min showed obvious inhibition of tumor growth (Figure 4b and Supporting Information, Figure S18). Other groups, such as those injected with DOX, showed a lower level of tumor growth inhibition. Furthermore, histological analysis indicated UCNPs-LA$_{Azo}$BC$_{Azo}$/DOX-TAT-HA treatment led to massive cell remission after NIR irradiation (Figure 4c), confirming its better inhibition effect on tumor growth. More importantly, no apparent variation in body weight was observed for all experiment groups (Supporting Information, Figure S19), even the mice treated with UCNPs-LA$_{Azo}$BC$_{Azo}$/DOX-TAT-HA, and the liver, heart, lung, spleen, and kidney did not show obvious pathological abnormalities (Supporting Information, Figure S20), indicating good tumor-targeting capability and little side-effects of the DNA–azo nanopump.

In conclusion, we present a new paradigm for enhanced intracellular drug release and anticancer therapy using a newly designed DNA–azo nanopump. The nanopump can be conveniently prepared by assembling azo-functionalized DNA strands on UCNPs and fueled with upconversion luminescence for rapid and efficient drug release. As a controlled delivery system, the anticancer drug DOX can be loaded on the formed DNA helix, and both cancer-cell targeting and nuclear localization have been used to improve the therapeutic efficacy. Under 980 nm NIR irradiation, the continuous rotation-inversion movement of azo molecules induces DNA hybridization and dehybridization for controllable release of DOX. The delivery system showed good biocompatibility and excellent performance in both cellular and in vivo therapy. We envision that this upconversion-luminescence-fueled DNA–azo nanopump could improve the chemotherapeutic outcomes of solid tumors in clinical applications.

Acknowledgements

We gratefully acknowledge the National Natural Science Foundation of China (21635005, 21605083, 21827812, 21890741, 21771103, 21974064), National Research Foundation for Thousand Youth Talents Plan of China, Natural Science Foundation of Jiangsu Province (BK 20160644, BK 20160639), State Key Laboratory of Analytical Chemistry for Life Science (5431ZZXM1806), Specially-appointed Professor Foundation of Jiangsu Province, and Program for Innovative Talents and Entrepreneurs of Jiangsu Province.

Conflict of interest

The authors declare no conflict of interest.

Keywords: antitumor agents · azobenzene · DNA nanotechnology · drug delivery · upconversion nanoparticles

How to cite: *Angew. Chem. Int. Ed.* **2019**, *58*, 18207–18211
Angew. Chem. **2019**, *131*, 18375–18379

[1] a) I. Keklikoglou, C. Cianciaruso, E. Guc, M. L. Squadrito, L. M. Spring, S. Tazzyman, L. Lambein, A. Poissonnier, G. B. Ferraro, C. Baer, A. Cassara, A. Guichard, M. L. Iruela-Arispe, C. E. Lewis, L. M. Coussens, A. Bardia, R. K. Jain, J. W. Pollard, M. De Palma, *Nat. Cell Biol.* **2019**, *21*, 190 – 202; b) P. Carlson, A. Dasgupta, C. A. Grzelak, J. Kim, A. Barrett, I. M. Coleman, R. E. Shor, E. T. Goddard, J. Dai, E. M. Schweitzer, A. R. Lim, S. B. Crist, D. A. Cheresh, P. S. Nelson, K. C. Hansen, C. M. Ghajar, *Nat. Cell Biol.* **2019**, *21*, 238 – 250.

[2] a) O. S. Fenton, K. N. Olafson, P. S. Pillai, M. J. Mitchell, R. Langer, *Adv. Mater.* **2018**, *30*, 1705328; b) M. Karimi, A. Ghasemi, P. Sahandi Zangabad, R. Rahighi, S. M. Moosavi Basri, H. Mirshekari, M. Amiri, Z. Shafaei Pishabad, A. Aslani, M. Bozorgomid, D. Ghosh, A. Beyzavi, A. Vaseghi, A. R. Aref, L. Haghani, S. Bahrami, M. R. Hamblin, *Chem. Soc. Rev.* **2016**, *45*, 1457 – 1501.

[3] a) C. H. Lu, I. Willner, *Angew. Chem. Int. Ed.* **2015**, *54*, 12212 – 12235; *Angew. Chem.* **2015**, *127*, 12380 – 12405; b) X. Xu, J. Wu, Y. Liu, M. Yu, L. Zhao, X. Zhu, S. Bhasin, Q. Li, E. Ha, J. Shi, O. C. Farokhzad, *Angew. Chem. Int. Ed.* **2016**, *55*, 7091 – 7094; *Angew. Chem.* **2016**, *128*, 7207 – 7210.

[4] a) T. Zhao, D. Zhao, P. Wang, Q. Li, A. A. Al-Khalaf, W. N. Hozzein, F. Zhang, X. Li, *Angew. Chem. Int. Ed.* **2018**, *57*, 2611 – 2615; *Angew. Chem.* **2018**, *130*, 2641 – 2645; b) H. Z. Kang, H. P. Liu, J. A. Phillips, Z. H. Cao, Y. Kim, Y. Chen, Z. Y. Yang, J. W. Li, W. H. Tan, *Nano Lett.* **2009**, *9*, 2690 – 2696; c) J. Park, L. B. Sun, Y. P. Chen, Z. Perry, H. C. Zhou, *Angew. Chem. Int. Ed.* **2014**, *53*, 5842 – 5846; *Angew. Chem.* **2014**, *126*, 5952 – 5956.

[5] H. Yan, C. Teh, S. Sreejith, L. L. Zhu, A. Kwok, W. Q. Fang, X. Ma, K. T. Nguyen, V. Korzh, Y. L. Zhao, *Angew. Chem. Int. Ed.* **2012**, *51*, 8373 – 8377; *Angew. Chem.* **2012**, *124*, 8498 – 8502.

[6] T. Ogoshi, S. Takashima, T. A. Yamagishi, *J. Am. Chem. Soc.* **2018**, *140*, 1544 – 1548.

[7] a) L. Peng, M. X. You, Q. Yuan, C. C. Wu, D. Han, Y. Chen, Z. H. Zhong, J. G. Xue, W. H. Tan, *J. Am. Chem. Soc.* **2012**, *134*, 12302 – 12307; b) H. R. Culver, J. R. Clegg, N. A. Peppas, *Acc. Chem. Res.* **2017**, *50*, 170 – 178.

[8] a) J. Croissant, M. Maynadier, A. Gallud, H. Peindy N'dongo, J. L. Nyalosaso, G. Derrien, C. Charnay, J. O. Durand, L. Raehm, F. Serein-Spirau, N. Cheminet, T. Jarrosson, O. Mongin, M. Blanchard-Desce, M. Gary-Bobo, M. Garcia, J. Lu, F. Tamanoi, D. Tarn, T. M. Guardado-Alvarez, J. I. Zink, *Angew. Chem. Int. Ed.* **2013**, *52*, 13813 – 13817; *Angew. Chem.* **2013**, *125*, 14058 – 14062; b) M. Fujiwara, M. Akiyama, M. Hata, K. Shiokawa, R. Nomura, *ACS Nano* **2008**, *2*, 1671 – 1681; c) W. Xiao, P. Wang, C. Ou, X. Huang, Y. Tang, M. Wu, W. Si, J. Shao, W. Huang, X. Dong, *Biomaterials* **2018**, *183*, 1 – 9.

[9] a) X. Ai, L. Lyu, Y. Zhang, Y. Tang, J. Mu, F. Liu, Y. Zhou, Z. Zuo, G. Liu, B. Xing, *Angew. Chem. Int. Ed.* **2017**, *56*, 3031 – 3035; *Angew. Chem.* **2017**, *129*, 3077 – 3081; b) D. Yang, P. Ma, Z. Hou, Z. Cheng, C. Li, J. Lin, *Chem. Soc. Rev.* **2015**, *44*, 1416 – 1448; c) X. Li, Z. Guo, T. Zhao, Y. Lu, L. Zhou, D. Zhao, F. Zhang, *Angew. Chem. Int. Ed.* **2016**, *55*, 2464 – 2469; *Angew. Chem.* **2016**, *128*, 2510 – 2515.

[10] a) J. Liu, W. Bu, L. Pan, J. Shi, *Angew. Chem. Int. Ed.* **2013**, *52*, 4375 – 4379; *Angew. Chem.* **2013**, *125*, 4471 – 4475; b) C. Yao, P. Wang, X. Li, X. Hu, J. Hou, L. Wang, F. Zhang, *Adv. Mater.* **2016**, *28*, 9341 – 9348.

[11] J. Wang, H. Wang, H. Wang, S. He, R. Li, Z. Deng, X. Liu, F. Wang, *ACS Nano* **2019**, *13*, 5852 – 5863.

[12] L. Y. Li, P. L. Hao, P. Wei, L. M. Fu, X. C. Ai, J. P. Zhang, J. Zhou, *Biomaterials* **2017**, *136*, 43 – 55.

[13] W. C. Liao, C. H. Lu, R. Hartmann, F. A. Wang, Y. S. Sohn, W. J. Parak, I. Willner, *ACS Nano* **2015**, *9*, 9078 – 9086.

[14] W. Fan, B. Shen, W. Bu, X. Zheng, Q. He, Z. Cui, K. Zhao, S. Zhang, J. Shi, *Chem. Sci.* **2015**, *6*, 1747 – 1753.

[15] a) L. Pan, Q. He, J. Liu, Y. Chen, M. Ma, L. Zhang, J. Shi, *J. Am. Chem. Soc.* **2012**, *134*, 5722 – 5725; b) L. Pan, J. Liu, J. Shi, *Adv. Funct. Mater.* **2014**, *24*, 7318 – 7327.

[16] W. Chen, G. Luo, Q. Lei, S. Hong, W. Qiu, L. Liu, S. Cheng, X. Zhang, *ACS Nano* **2017**, *11*, 1419 – 1431.

[17] a) W. Chen, G. Luo, W. Qiu, Q. Lei, S. Hong, S. Wang, D. Zheng, C. Zhu, X. Zeng, J. Feng, S. Cheng, X. Zhang, *Small* **2016**, *12*, 733 – 744; b) Q. Hu, W. Sun, Y. Lu, H. N. Bomba, Y. Ye, T. Jiang, A. J. Isaacson, Z. Gu, *Nano Lett.* **2016**, *16*, 1118 – 1126.

[18] T. Jiang, Z. Zhang, Y. Zhang, H. Lv, J. Zhou, C. Li, L. Hou, Q. Zhang, *Biomaterials* **2012**, *33*, 9246 – 9258.

[19] Y. Zhang, K. Ren, X. Zhang, Z. Chao, Y. Yang, D. Ye, Z. Dai, Y. Liu, H. Ju, *Biomaterials* **2018**, *163*, 55 – 66.

[20] C. Homann, L. Krukewitt, F. Frenzel, B. Grauel, C. Würth, U. Resch-Genger, M. Haase, *Angew. Chem. Int. Ed.* **2018**, *57*, 8765 – 8769; *Angew. Chem.* **2018**, *130*, 8901 – 8905.

[21] J. Wang, T. Wei, X. Li, B. Zhang, J. Wang, C. Huang, Q. Yuan, *Angew. Chem. Int. Ed.* **2014**, *53*, 1616 – 1620; *Angew. Chem.* **2014**, *126*, 1642 – 1646.

[22] F. Huang, W. C. Liao, Y. S. Sohn, R. Nechushtai, C. H. Lu, I. Willner, *J. Am. Chem. Soc.* **2016**, *138*, 8936 – 8945.

[23] K. R. Kim, D. R. Kim, T. Lee, J. Y. Yhee, B. S. Kim, I. C. Kwon, D. R. Ahn, *Chem. Commun.* **2013**, *49*, 2010 – 2012.

[24] P. Zhang, C. Wang, J. Zhao, A. Xiao, Q. Shen, L. Li, J. Li, J. Zhang, Q. Min, J. Chen, H. Y. Chen, J. J. Zhu, *ACS Nano* **2016**, *10*, 3637 – 3647.

[25] Y. Zhu, M. Fujiwara, *Angew. Chem. Int. Ed.* **2007**, *46*, 2241 – 2244; *Angew. Chem.* **2007**, *119*, 2291 – 2294.

[26] a) S. S. Agasti, A. Chompoosor, C. C. You, P. Ghosh, C. K. Kim, V. M. Rotello, *J. Am. Chem. Soc.* **2009**, *131*, 5728 – 5729; b) A. G. Skirtach, A. M. Javier, O. Kreft, K. Kohler, A. P. Alberola, H. Mohwald, W. J. Parak, G. B. Sukhorukov, *Angew. Chem. Int. Ed.* **2006**, *45*, 4612 – 4617; *Angew. Chem.* **2006**, *118*, 4728 – 4733; c) M. F. Bédard, S. Sadasivan, G. B. Sukhorukov, A. Skirtach, *J. Mater. Chem.* **2009**, *19*, 2226 – 2233.

[27] a) M. Ye, Y. Han, J. Tang, Y. Piao, X. Liu, Z. Zhou, J. Gao, J. Rao, Y. Shen, *Adv. Mater.* **2017**, *29*, 1702342; b) L. Qiu, T. Chen, I. Ocsoy, E. Yasun, C. Wu, G. Zhu, M. You, D. Han, J. Jiang, R. Yu, W. Tan, *Nano Lett.* **2015**, *15*, 457 – 463; c) T. Zhaoxu, Q. Haishi, Y. Yuting, G. Guy, C. Wei, A. Mohsen, H. Rainer, *Angew. Chem. Int. Ed.* **2018**, *57*, 2611 – 2615; *Angew. Chem.* **2018**, *130*, 2641 – 2645.

[28] a) L. Yang, Z. Wang, J. Wang, W. Jiang, X. Jiang, Z. Bai, Y. He, J. Jiang, D. Wang, L. Yang, *Nanoscale* **2016**, *8*, 6801 – 6809; b) H. Wang, Y. Li, H. Bai, J. Shen, X. Chen, Y. Ping, G. Tang, *Adv. Funct. Mater.* **2017**, *27*, 1700339.

[29] X. Huang, Y. Lai, G. B. Braun, N. O. Reich, *Small* **2017**, *13*, 1602473.

Manuscript received: August 6, 2019
Revised manuscript received: October 2, 2019
Accepted manuscript online: October 4, 2019
Version of record online: October 24, 2019

